NANO LETTERS

2007
Vol. 7, No. 6
1521−1525

# Getting to the Core of the Problem: Origin of the Luminescence from (Mg,Zn)O Heterostructured Nanowires

**Richard A. Rosenberg* and Gopal K. Shenoy**

*Argonne National Laboratory, 9700 South Cass Avenue, Argonne, Illinois 60439*

**Matthew F. Chisholm**

*Oak Ridge National Laboratory, Oak Ridge, Tennessee 37831*

**Li-Chia Tien, David Norton, and Steven Pearton**

*Department of Materials Science and Engineering, University of Florida, Gainesville, Florida 32611*

*Received February 5, 2007; Revised Manuscript Received April 25, 2007*

**ABSTRACT**

**We have measured the time-resolved, X-ray excited optical luminescence spectra from two types of $Mg_xZn_{(1-x)}O$ core−shell, heterostructured nanowires: type I, with a small *x*, wurtzite core, encased in a larger *x*, wurtzite sheath; and type II, with a wurtzite core ($x \sim 0$), encased in a rock-salt sheath ($x > 0.62$). By monitoring the X-ray energy dependence of the various luminescence peaks, we have determined the local environment of the sites where these peaks originate.**

Luminescence is one of the most important means for determining the electronic properties of nanostructures. For hetero-nanostructures the emission can become quite complex due to the presence of multiple phases, interfaces, and surfaces. Analysis of the luminescence spectra can present a challenge, particularly when the structures are differentiated not by chemical composition but by multiple phases. In the present paper we demonstrate how time-resolved X-ray excited optical luminescence (XEOL) may utilized to understand the complicated emission spectra from (Mg,Zn)O core−shell hetero-nanostructures.

Due to its wide band gap and high exciton binding energy (60 meV), ZnO has potential for a wide range of optoelectronic applications. ZnO thin films have found a wide range of applications including catalysis, varistors, surface acoustic wave devices, sensors, and transducers.[1,2] It can form a wide variety of nanostructures, including wires, rods, belts, combs, rings, and helixes/springs.[3−5] The discovery of room-temperature UV lasing[6] in ZnO nanowires has stimulated a considerable effort into understanding its optical properties.

As ZnO is alloyed with Mg to form $Mg_xZn_{(1-x)}O$, its band gap increases from 3.3 to 7.8 eV as *x* goes from 0 to 1. For Mg concentrations less than 37% the structure is hexagonal, and when it exceeds 62%, the structure is cubic with a lattice constant close to MgO. In the region between 37% and 62% Mg the structure is mixed with undefined energy band gaps.[7] The ability to tune the energy band gap over such a wide range has led to a great deal of interest in the properties of both thin films and nanostructures.

The growth and properties of one-dimensional ZnO-based homo- and heterostructures has recently been reviewed.[8] In addition to lasers, such structures may be used as gas and chemical sensors, MOSFETS, and spin-polarized light sources (when doped with transition metals). In this paper our focus is on one-dimensional (1-D) cored nanowire heterostructures of (Mg,Zn)O in which the chemical modulation extends radially. In particular, two types of heterostructures were investigated for their luminescent properties. The first (type I) consisted of a wurtzite core with a low Mg concentration encased in a wurtzite shell with a higher Mg concentration, while the second (type II) had a wurtzite core with little or no Mg surrounded by a rock salt structured shell with a high Mg concentration. To understand the optical properties and electronic structure of these complex nanostructures, it is essential to have tools with unique capabilities. In the present paper we utilize XEOL to probe the nature of the chemical environments responsible for a specific luminescence peak from these nanowires.

* Corresponding author: e-mail, rar@aps.anl.gov; phone, 630-252-6112; fax, 630-252-9350.

10.1021/nl0702923 CCC: $37.00 
**Published on Web 05/27/2007**

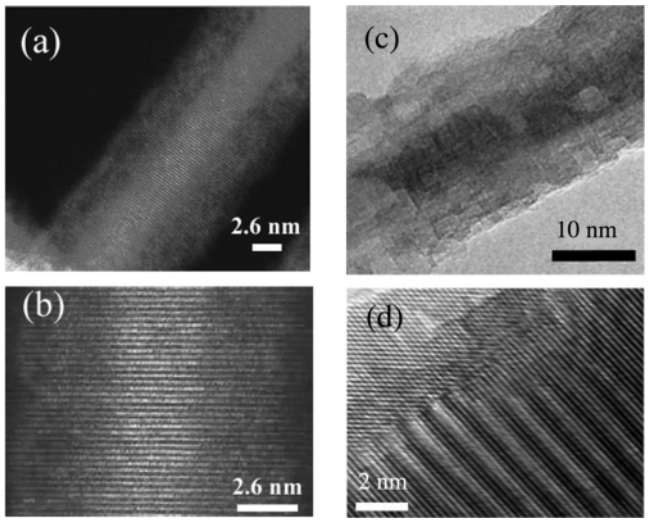


**Figure 1.** High-resolution Z-STEM images of type I (a, b) and type II (c, d) nanorods.

XEOL has been shown to be a powerful tool for investigating the local chemical environment of a site that gives rise to a particular luminescent band.[9] Recently we have used XEOL to understand the nature of the band gap and defect luminescence from ZnO nanowires[10] and identify the origin of the luminescence from Si−CdSe nano-heterostructures.[11]

Time-resolved XEOL measurements show that type I structures have a very intense, short-lived band gap luminescence with very little defect-related emission. Type II structures have much weaker luminescence with high contributions from long-lived defect sites. X-ray absorption near-edge structure (XANES) measurements using the appropriate luminescence signals reveal the sites responsible for the emission. The band gap luminescence from both type I and type II structures emanates from the core, while the defect luminescence from type II originates in the shell.

The experiments were performed using soft X-rays from beamline 4-ID-C at the Advanced Photon Source. This facility provides intense, tunable, pulsed (80-ps width, 153-ns period) radiation in the range 500−3000 eV. The X-rays irradiated the sample at normal incidence, and the emitted optical photons were extracted at 45° using a condenser lens and then focused on the entrance slit of a 0.3-m monochromator. A cooled photomultiplier tube was used to detect the dispersed photons, which were then processed using time-correlated single-photon counting techniques. The sample was mounted on a manipulator located in an ultrahigh vacuum end station.

Samples were prepared at the University of Florida using a Ag catalyst enhanced molecular beam epitaxy approach.[12] The results presented here were obtained using rods of ∼50 nm diameter. In all cases the substrate was Si and the synthesis resulted in randomly oriented nanostructures.

Parts a and b of Figure 1 show high-resolution Z-STEM images of a type I nanorod. The lattice image for the nanorod specimen indicates that the rod is crystalline with the wurtzite crystal structure maintained throughout the cross section. The

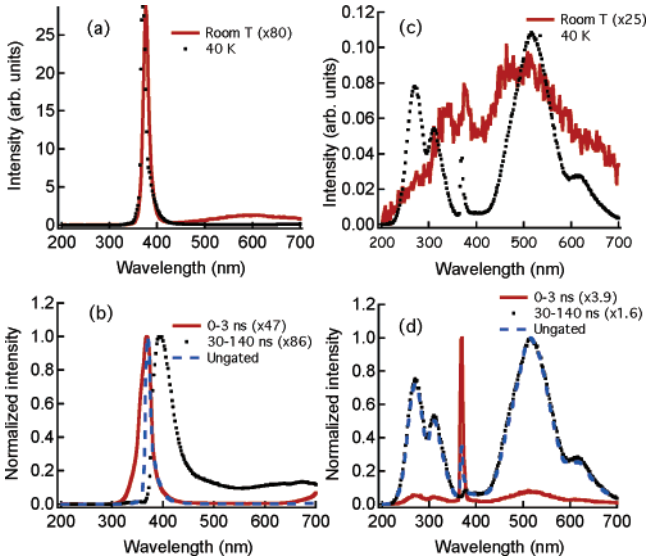


**Figure 2.** Optical luminescence spectra following irradiation with 1000 eV X-rays: (a) type I at room temperature (solid, red) and 40 K (dots, black); (b) type I, 40 K, with time gates of 0−3 ns (solid, red), 30−140 ns (dots, black), and ungated (dashed, blue); (c) type II at room temperature (solid, red) and 40 K (dots, black); (d) type II, 40 K, with time gates of 0−3 ns (solid, red), 30−140 ns (dots, black), and ungated (dashed, blue). The same arbitrary unit scale was used for the *y*-axis in (a) and (c), so intensities may be compared. For (b) and (d) the intensities of the spectra were normalized to the maximum for each curve.

*c*-axis is oriented along the long axis of the rod. The higher contrast for the center core region clearly indicates a higher cation atomic mass. The structures consist of a zinc-rich $Zn_{1-x}Mg_xO$ core (small $x$) surrounded by a $Zn_{1-y}Mg_yO$ (large $y$) sheath containing higher Mg content. Figure 1c shows a transmission electron microscopy (TEM) image of a type II nanowire, displaying a difference in brightness intensity between the core and sheath regions. This image was obtained without the objective aperture in order to minimize any diffraction contrast. The contrast across the diameter of the nanowire is predominantly mass contrast, reflecting a difference in average atomic number ($Z$) of the core and sheath region. The darker core region contains more Zn, the lighter sheath region more Mg. The high-resolution image shown in Figure 1d indicates a radial heterostructured nanowire in which the interface between the sheath and core is epitaxial despite the discontinuity in crystal structure and symmetry. The lower-right region of the image is the core, while the upper-left region is the sheath. Growth of the core yields the rod axis along the *c*-axis direction of the hexagonal ZnO. For the (Mg,Zn)O sheath, the (200), $(1\bar{1}1)$, and $(11\bar{1})$ planes match those of the rock salt structure, according to the lattice spacing and angle between planes. Note that the lattice mismatch between the (Mg,Zn)O (200) planes and the ZnO (0002) planes produces regularly spaced interfacial edge dislocations. In addition selective area diffraction measurements show single-crystal patterns that correspond to the wutzite and cubic rock salt structures.[8,13]

XEOL spectra of both types of structures are shown in Figure 2. In (a) are shown spectra of a type I structure at both room temperature and ∼40 K. The spectra are domi-

nated by an intense band-edge exciton peak at ∼367 nm (3.37 eV) that shifts to lower wavelength and increases in intensity as the temperature is lowered. Figure 2b shows the ungated 40 K spectrum plus spectra obtained with two different time gates, 0−3 ns and 30−140 ns. The 367 nm, band-edge peak dominates the short time-gate spectrum, indicating that it has a relatively short lifetime. It is broadened toward lower wavelengths, which indicates the presence of unresolved short-lifetime levels, possibly band-edge exitons emanating from the higher band gap shell. Attempts to measure the lifetime were not successful, indicating that it is less than the time response of our system (∼1 ns). The peak at 395 nm that appears in the long time-gated spectrum is probably due to emission from donor acceptor states.[2,14]

Dramatic changes are seen in the XEOL spectra of type II nanowires shown in parts c and d of Figure 2. At room temperature a very weak band edge (∼370 nm) peak is observed which is nestled between broad, defect-related structures. Upon cooling to 40 K all the peaks increase in intensity and the broad peaks become more defined, with peak wavelengths of 270, 310, 525, and 620 nm. On the basis of the intensity of the second-order, band-edge peak at ∼740 nm (not shown), we estimate that ∼20% of the area in the peaks at 525 and 620 nm could be due to second-order contribution from the peaks at 270 and 310 nm. Thus, all the intensity of the 620 nm peak and ∼15% of the 525 nm peak could be due to second-order light. The time-gated spectra shown in Figure 2d indicate that all the broad peaks have relatively long lifetimes while the band-edge exciton has a short lifetime (<1 ns). The lifetimes of all the broad peaks were too large to be measured due to the limitation imposed by the 153 ns gap between pulses. Such long lifetimes are typically found in defect-related peaks.[15]

The published cathodoluminescence spectrum of cubic MgZnO shows peaks at 2.2, 3.55, and 3.74 eV (563, 349, and 331 nm).[16] There have several reports on luminescence from cubic MgO which reveal peak energies ranging from 250 to 730 nm.[17−19] On the basis of the assignments given in these previous studies we speculate that the 270 and 310 nm emissions seen in Figure 2d are due to the recombination of an electron with a $V^-$ center (a hole trap on an oxygen next to a magnesium ion vacancy), while the 525 nm peak is due to transitions of an F center located at an oxygen vacancy.

The relative intensity of the exciton peak in the type I structure is over 750 times more than its counterpart in the type II structure. The defects, evidenced by the broad, long-lived states in Figure 2c, might be expected to provide quenching sites for the exciton state. However, results from the X-ray energy dependence of the exciton and defect luminescence yields (see below) indicate that the exciton state lies in the core while the defects are located in the shell. Therefore, the defects that yield the structure in Figure 2c should not directly be involved in quenching the exciton state. However, there are other defects that could be involved, such as the edge dislocations mentioned previously.[8] Furthermore, it is evident from the TEM images in Figure 1 that both the core−shell interface and the surface of type I structures are

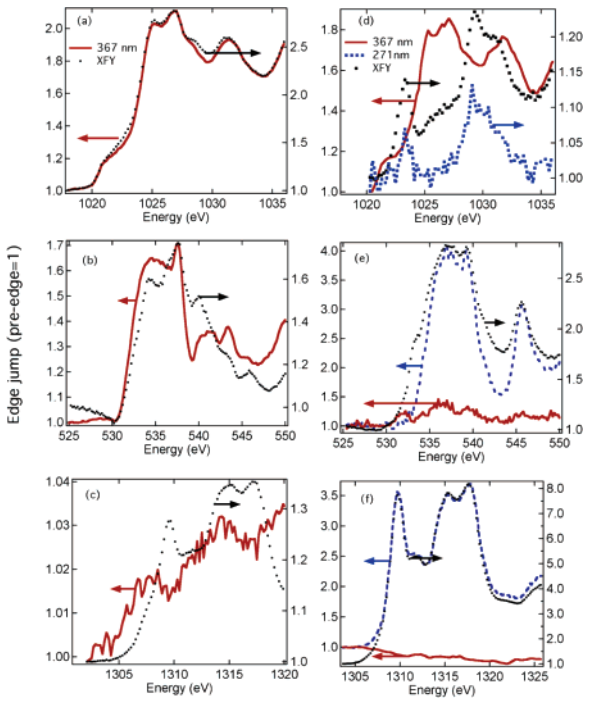


**Figure 3.** X-ray energy excitation scans at the Zn L, O K, and Mg K edges for type I (a−c) and II (d−f) structures. The intensity is given in terms of the "edge jump", where the low-energy, pre-edge region is normalized to 1.

much smoother than their type II counterparts. Interfacial and surface defects would also be expected to play a role in quenching the luminescence. Finally, it should be noted that the shell in type I structures contains a relatively high concentration of Mg compared to the core, so the band gap of the shell component is higher than that of the core. The shell thus serves to passivate the core surface and contain the exciton in a manner similar to the way ZnS overlayers passivate CdSe nanodots.[20] Such systems might be expected to be good candidates for lasing.

There is no evidence in parts c and d of Figure 2 for a sharp, short-lived exciton state at shorter wavelengths than the 270 nm peak for the type II structure. This could be due to 100% quenching of the exciton state by defects or that the exciton state emission is beyond the detection limits of the optical spectrometer (<∼200 nm). This implies that the band gap for the sheath region of the type II structure is >4.6 eV, which is reasonable, based on the band gap of rock salt $Mg_xZn_{(1-x)}O$ ($x > 0.62$).[7]

As the X-ray energy is scanned through the core level binding energy of a particular atom in the nanostructure (Zn L, O K, and Mg K), an electron is excited from the core level to previously unoccupied states in the conduction band. De-excitation of the electron can gives rise to XEOL. A change in XEOL signal, or edge-jump, reflects the XANES spectrum which yields chemical and structural information on the luminescing region.

The XANES spectra obtained by measuring XEOL signals at various optical luminescence channels for type I (a−c) and II (d−f) structures are shown in Figure 3. We have also shown the X-ray absorption spectrum, which is proportional

to the X-ray fluorescence yield (XFY). One observes striking differences in XANES measured in various luminescence channels and the XFY. The intensity is given in terms of the "edge jump", where the low energy, pre-edge region is normalized to 1. This allows for a quantitative comparison among the various channels.

Results obtained for type I structures at the Zn L edge are shown in Figure 3a. The X-ray absorption (dotted, black), as given by the total XFY, as well as the 367 nm luminescence spectrum (solid, red) are similar to that reported previously for wurtzite ZnO nanowires.[10,21,22] This is not surprising, since the local sites that give rise to the band-edge luminescence should have a wurtzite structure. Dramatic differences among the various channels are seen in the Zn L excitation scans of type II structures (Figure 3d). The band-edge (367 nm) luminescence spectrum (solid, red) is similar to that from the type I, wurtzite structure (Figure 3a). However, the spectrum for the 270 nm (dashed, blue), as well as the 310 and 525 nm (not shown but similar to that from 270 nm), defect luminescence is strikingly different. It is dominated by two peaks at 1023 and 1029 eV that are also seen in the electron energy loss measurements of Zn-doped (10%) MgO which also shows similarly shaped peaks separated by 6 eV.[23] Calculations show that the Zn $L_3$ XANES of rock salt ZnO is dominated by two peaks separated by ~8 eV,[24] which correspond to the two peaks separated by 6 eV in the experimental spectrum. Recent Zn $L_{2,3}$ X-ray absorption measurements of of MgO−ZnO solid solution (2.5 mol %) having a rock salt structure also show the same peak structure.[25] The simulations of XANES spectra indicate that the experimental data represent disordered phase around Zn atoms in this solid solution.[25] These observations convincingly show that the defect luminescence originates in the rock salt shell of the type II nanowire. The XFY curve is a reflection of the overall nanowire structure and should contain contributions from the wurtzite core. Since more X-rays are absorbed in the outer, shell region, the XFY is dominated by the rock salt contribution.

Results obtained for type I structures at the O K edge are shown in Figure 3b. The X-ray absorption, as given by the total XFY, spectrum is similar to that reported previously for ZnO nanowires.[21,22,24] However, striking differences are seen between the band-edge yield and the XFY curve. There is an enhancement of the feature at 533 eV relative to that at 537 eV in the band-edge (367 nm) excitation curve. As explained previously,[10] the enhancement in the band-edge luminescence at 533 eV is due to the localized nature of the excitation, which selectively excites O 1s to $p_z$ states that project strongly along the *c*-axis of the nanocrystal, which is also the symmetry axis for the exciton state. Radiative de-excitation of the $p_{x,y}$ states at 537 eV is much less efficient since these states do not overlap strongly with the radiating dipole. The enhancement of the luminescence yield is seen when there is strong overlap between the dipole formed by core-level excitation and that of the luminescence.

O K edge spectra from the type II structure are shown in Figure 3e. The XFY spectrum should be a weighted average of that of the wurtzite ZnO (as in Figure 3a) core and the rock salt (Mg,Zn)O shell. Calculations show that the O K XANES of rock salt ZnO is dominated by two peaks separated by ~3 eV;[24] these peaks correspond to the two peaks in the experimental spectra at 536.8 and 539.4 eV. Similar structure is also seen in the X-ray absorption spectrum of MgO thin films.[26,27] The shoulder at 533 eV in the XFY spectrum originates in the wurtzite core. This shoulder is absent in the yield curve of the 270 nm defect level, which supports the rock salt shell assignment based on the Zn L edge results in Figure 3d. The XANES curve for the 367 nm level is relatively weak. This is due to (1) quenching of the excitation in the nanowire core by interfacial defects and (2) absorption of potential O K excitation X-rays by the oxygen in the shell region.

Results at the Mg K edge are shown in Figure 3c for type I and in Figure 3f for type II structures. The XFY curve in Figure 3c is similar to the recently reported X-ray absorption spectra of Mg-doped wurtzite ZnO nanowires,[28] while the yield of the 367 nm, band-edge excitons shows dips at the positions of the peaks in the XRF spectrum. These dips arise because there is more Mg in the shell region than in the core, so impinging X-rays are preferentially adsorbed in the shell. Furthermore, this implies that excitations in the shell region are not effective at producing excitons, and therefore the excitons are localized to the core region. Thus, the shell region does not emit (is dark). The XRF and 270 nm yield curves for type II structures in Figure 3f are very similar to that obtained from cubic, MgO thin films.[26,27] This correspondence further supports the assignment of the origin of the defect level emission to the Mg-rich, rock salt shell. In contrast the 367 nm, band-edge luminescence yield in Figure 3f shows no structure at the Mg K edge. This is reasonable since there is little if any Mg in the core of the type II structure.

In summary we have measured the time-resolved, X-ray excited optical luminescence spectra from two types of $Mg_xZn_{(1-x)}O$ core−shell, heterostructured nanowires: type I, with a small *x*, wurtzite core, encased in a larger *x*, wurtzite sheath; and type II, with a wurtzite core ($x \sim 0$), encased in a rock salt sheath ($x > 0.62$). The luminescence spectrum from type I is dominated by a very intense, short-lived, band-edge exciton peak. For the type II structure, the exciton emission is much weaker, and there is also emission from several long-lived defect levels. The X-ray energy dependence of the various emitting states shown in Figure 3 is an excellent demonstration of the site and excitation-channel selectivity of XEOL. From these results we have determined that for both types of structures the band-edge exciton state is localized in the core, while the defect levels in type II structures are localized in the sheath region. The shell in type I structures is dark (does not emit). These results should prove of great value to future nanoengineers who need to integrate such structures into functional devices.

**Acknowledgment.** Use of the Advanced Photon Source was supported by the U.S. Department of Energy, Office of Science, Office of Basic Energy Sciences, under Contract No. DE-AC02-06CH11357. The work at Oak Ridge National Laboratory sponsored by the Office of Basic Energy Sci-

ences, U.S. Department of Energy, under contract managed and operated by UT-Battelle, LLC. The work at UF was supported by the National Science Foundation (DMR 0400416, 0305228, Dr.L.Hess). The authors at UF also acknowledge the Major Analytical Instrumentation Center, Department of Materials Science and Engineering, University of Florida.

## References

(1) Pearton, S. J.; Norton, D. P.; Ip, K.; Heo, Y. W.; Steiner, T. *J. Vac. Sci. Technol., B* **2004**, *22*, 932.
(2) Ozgur, U.; Alivov, Y. I.; Liu, C.; Teke, A.; Reshchikov, M. A.; Dogan, S.; Avrutin, V.; Cho, S. J.; Morkoc, H. *J. Appl. Phys.* **2005**, *98*, 041301.
(3) Wang, Z. L. *J. Phys. Condens. Matter* **2004**, *16*, R829.
(4) Wang, Z. L. *ZnO Bulk, Thin Films and Nanostructures*; Jagadish, C., Pearton, S. J., Eds.; Elsevier: Amsterdam, 2006.
(5) Zou, B. S.; Liu, R.; Wang, F.; Pan, A.; Cao, L.; Wang, Z. L. *J. Phys. Chem. B* **2006**, *110*, 12865.
(6) Huang, M. H.; Mao, S.; Feick, H.; Yan, H.; Wu, Y.; Kind, H.; Weber, E.; Russo, R.; Yang, P. *Science* **2001**, *292*, 1897.
(7) Yang, W.; Hullavarad, S. S.; Nagaraj, B.; Takeuchi, I.; Sharma, R. P.; Venkatesan, T.; Vispute, R. D.; Shen, H. *Appl. Phys. Lett.* **2003**, *82*, 3424.
(8) Heo, Y. W.; Norton, D. P.; Tien, L. C.; Kang, B. S.; Ren, F.; Pearton, S. J.; LaRoche, J. R. *Mater. Sci. Eng. R* **2004**, *47*, 1.
(9) Rogalev, A.; Goulon, J. X-ray Excited Optical Luminescence Spectroscopies. In *Chemical Applications of Synchrotron Radiation, Part II: X-ray Applications*; Sham, T. K., Ed.; World Scientific Publishing Co.: Singapore, 2002; p 707.
(10) Rosenberg, R. A.; Shenoy, G. K.; Tien, L. C.; Norton, D.; Pearton, S.; Sun, X. H.; Sham, T. K. *Appl. Phys. Lett.* **2006**, *89*, 093118.
(11) Rosenberg, R. A.; Shenoy, G. K.; Sun, X. H.; Sham, T. K. *Appl. Phys. Lett.* **2006**, *89*, 243102.
(12) Heo, Y. W.; Varadarajan, V.; Kaufman, M.; Kim, K.; Norton, D. P.; Ren, F.; Fleming, P. H. *Appl. Phys. Lett.* **2002**, *81*, 3046.
(13) Heo, Y. W.; Kaufman, M.; Pruessner, K.; Siebein, K. N.; Norton, D. P.; Ren, F. *Appl. Phys. A* **2005**, *80*, 263.
(14) Thonke, K.; Gruber, T.; Teofilov, N.; Schonfelder, R.; Waag, A.; Sauer, R. *Physica B* **2001**, *308*−*310*, 945.
(15) Leverenz, H. W. *An Introduction to Luminescence of Solids*; John Wiley and Sons, Inc.: New York, 1950.
(16) Baranov, A. N.; Solozhenko, V. L.; Chateau, C.; Bocquillon, G.; Petitet, J. P.; Panin, G. N.; Kang, T. W.; Shpanchenko, R. V.; Antipov, E. V.; Oh, Y. J. *J. Phys.*: *Condens. Matter* **2005**, *17*, 3377.
(17) Grant, J. L.; Cooper, R.; Zeglinski, P.; Boas, J. F. *J. Chem. Phys.* **1989**, *90*, 807.
(18) Rosenblatt, G. H.; Rowe, M. W.; Williams, G. P.; Williams, R. T.; Chen, Y. *Phys. Rev. B* **1989**, *39*, 10309.
(19) Williams, R. T.; Williams, J. W.; Turner, T. J.; Lee, K. H. *Phys. Rev. B* **1979**, *20*, 1687.
(20) Nirmal, M.; Brus, L. *Acc. Chem. Res.* **1999**, *32*, 407.
(21) Chiou, J. W.; Jan, J. C.; Tsai, H. M.; Bao, C. W.; Pong, W. F.; Tsai, M. H.; Hong, I. H.; Klauser, R.; Lee, J. F.; Wu, J. J.; Liu, S. C. *Appl. Phys. Lett.* **2004**, *84*, 3462.
(22) Guo, J.-H.; Vayssieres, I.; Persson, C.; Ahuja, R.; Johansson, B.; Nordgren, J. *J. Phys.*: *Condens. Matter* **2005**, *17*.
(23) Mizoguchi, T.; Yoshiya, M.; Li, J.; Oba, F.; Tanaka, I.; Adachi, H. *Ultramicroscopy* **2001**, *86*, 363.
(24) Mizoguchi, T.; Tanaka, I.; Yoshioka, S.; Kunisu, M.; Yamamoto, T.; Ching, W. Y. *Phys. Rev. B* **2004**, *70*, 045103.
(25) Tanaka, I.; Mizoguchi, T.; Yamamoto, T. *J. Am. Ceram. Soc.* **2005**, *88*, 2013.
(26) Lindner, T.; Sauer, H.; Engel, W.; Kambe, K. *Phys. Rev. B* **1986**, *33*, 22.
(27) Luches, P.; Addato, S. D.; Valeri, S.; Groppo, E.; Prestipino, C.; Lamberti, C.; Boscherini, F. *Phys. Rev. B* **2004**, *69*, 045412.
(28) Chiou, J. W.; Tsai, H. M.; Pao, C. W.; Kumar, K. P. K.; Ray, S. C.; Chien, F. Z.; Pong, W. F.; Tsai, M. H.; Chen, C. H.; Lin, H. J.; Wu, J. J.; Yang, M. H.; Liu, S. C.; Chiang, H. H.; Chen, C. W. *Appl. Phys. Lett.* **2006**, *89*, 043121.

NL0702923